$K_v2.1$ clusters on β-cell plasma membrane act as reservoirs that replenish pools of newcomer insulin granule through their interaction with syntaxin-3

Received for publication, March 4, 2018, and in revised form, March 9, 2018 Published, Papers in Press, March 16, 2018, DOI 10.1074/jbc.RA118.002703

Dafna Greitzer-Antes[‡1,2], Li Xie[‡1], Tairan Qin[‡], Huanli Xie[‡], Dan Zhu[‡], Subhankar Dolai[‡], Tao Liang[‡], Fei Kang[‡], Alexandre B. Hardy[‡], Yan He[§], Youhou Kang[‡], and Herbert Y. Gaisano[‡2]

From the [‡]Departments of Medicine and Physiology, University of Toronto, Toronto, Ontario M5S 1A8, Canada and the [§]Department of Epidemiology and Health Statistics, School of Public Health and Family Medicine, Capital Medical University, Beijing 100050, China

Edited by Jeffrey E. Pessin

The voltage-dependent K^+ (K_v) channel $K_v2.1$ is a major delayed rectifier in many secretory cells, including pancreatic β cells. In addition, $K_v2.1$ has a direct role in exocytosis at an undefined step, involving SNARE proteins, that is independent of its ion-conducting pore function. Here, we elucidated the precise step in exocytosis. We previously reported that syntaxin-3 (Syn-3) is the key syntaxin that mediates exocytosis of newcomer secretory granules that spend minimal residence time on the plasma membrane before fusion. Using high-resolution total internal reflection fluorescence microscopy, we now show that $K_v2.1$ forms reservoir clusters on the β-cell plasma membrane and binds Syn-3 via its C-terminal C1b domain, which recruits newcomer insulin secretory granules into this large reservoir. Upon glucose stimulation, secretory granules were released from this reservoir to replenish the pool of newcomer secretory granules for subsequent fusion, occurring just adjacent to the plasma membrane $K_v2.1$ clusters. C1b deletion blocked the aforementioned $K_v2.1$-Syn-3–mediated events and reduced fusion of newcomer secretory granules. These insights have therapeutic implications, as $K_v2.1$ overexpression in type-2 diabetes rat islets restored biphasic insulin secretion.

Voltage-dependent K^+ (K_v)[4] channel, $K_v2.1$ (*KCNB1*) was purported to account for most of the repolarization of pancreatic islet β-cell action potentials, and this has long been believed to be its major contribution to the regulation of insulin secretion (1, 2). However, more recent studies suggest that $K_v2.1$ may play a direct role in exocytosis, including neurons and other endocrine cells, by its interaction with soluble NSF attachment protein receptor (SNARE) protein syntaxin (Syn)-1A at the very proximal portion (C1a, aa 411–522) (3) of the cytoplasmic C terminus, and does not involve the ion-conducting pore (3–5). In support, disruption of this Syn-1A–binding site impaired depolarization-induced insulin secretory granule exocytosis in rodent and human β-cells (6). Whereas $K_v2.1$ binding to SNARE proteins forming complexes is reminiscent of SNARE-calcium channel excitosomes that were demonstrated to be the actual fusion apparatus (7, 8), membrane fusion *per se* is not likely to be the role of $K_v2.1$-SNARE complexes. In fact, the precise role of the $K_v2.1$-SNARE complex remains vague; it has been called a facilitator of exocytosis (4) or may be involved in vesicle recruitment (5). The $K_v2.1$ channel, through its distal C terminus, can insert into distinct microdomains in the plasma membrane and form clusters (9–11). Peculiarly, the majority of these $K_v2.1$ clusters were postulated to be electrically silent (12, 13); its role thus remains undefined but was postulated to serve as a stable cell surface platform for delivery of proteins or vesicle cargo to the cluster perimeter (14). Indeed, recent work has shown that $K_v2.1$ clusters play a role in forming membrane contact sites between the cortical endoplasmic reticulum and the plasma membrane (15).

We had elucidated the SNARE proteins that mediate the fusion of newcomer insulin secretory granules, which, unlike primed predocked secretory granules (16), approach the plasma membrane with minimal to no docking time before undergoing exocytotic fusion (17). The newcomer secretory granule SNARE proteins include cognate Syn-3 and VAMP8 (18, 19), distinct from the cognate SNARE partners Syn-1A and VAMP2 that mediate fusion of predocked secretory granules (16). β-cells secrete insulin in a biphasic manner in response to glucose, wherein predocked secretory granules contribute to the first phase (first 15 min) of glucose-stimulated insulin secretion (GSIS) (17). Newcomer secretory granules contribute to all of second-phase GSIS (after 15 min to several hours) and actually at least half of first-phase GSIS (17). The latter is of importance, as any strategy to increase recruitment of the larger number of newcomer secretory granules could potentially replace the loss of first-phase GSIS, a hallmark defect in type-2 diabetes

This work was supported by Canadian Institute of Health Research Grants MOP 69083 and MOP 86544. The authors declare that they have no conflicts of interest with the contents of this article.

This article contains Figs. S1–S4.

[1] Both authors contributed equally to this work.

[2] Supported by Banting and Best Diabetes Centre's Janssen Post-doctoral Fellowship of the University of Toronto.

[3] To whom correspondence should be addressed: Depts. of Medicine and Physiology, University of Toronto, Toronto, Ontario M5S 1A8, Canada. Tel.: 416-978-1526; Fax: 416-978-8765; E-mail: herbert.gaisano@utoronto.ca.

[4] The abbreviations used are: K_v, voltage-dependent K^+; Ca_v, voltage-dependent Ca^+; SNARE, soluble NSF attachment protein receptor; Syn, syntaxin; aa, amino acids; GSIS, glucose-stimulated insulin secretion; T2D, type-2 diabetes; Cm, cell membrane capacitance; fF, femtofarads; pF, picofarads; KD, knockdown; GK, Goto–Kakizaki; ROI, region of interest; TIRFM, total internal reflection fluorescence microscopy; EGFP, enhanced green fluorescent protein; GST, glutathione *S*-transferase; ANOVA, analysis of variance; AUC, area under the curve; Ad, adenovirus.

(T2D) patients and rodent models. Of note, the loss of first-phase GSIS has been postulated to be contributed in part by reduced levels of predocked secretory granule SNARE proteins (*i.e.* Syn-1A, VAMP2, and SNAP25) (20).

In this work, we have converged upon many of the questions raised above. We show that increasing $K_v2.1$ expression to form more $K_v2.1$ clusters on the plasma membrane of β-cells increases the recruitment of mainly newcomer secretory granules and also some predocked secretory granules. The newcomer secretory granules were guided and directed by $K_v2.1$ clusters before undergoing fusion that occurred adjacent to (rather than "right onto") $K_v2.1$ clusters. Syn-3 preferentially binds the $K_v2.1$-C1b domain to assemble into a complex that affects $K_v2.1$ channel activity. When the $K_v2.1$-C1b domain was deleted, recruitment of newcomer secretory granules to $K_v2.1$ clusters was disrupted, which consequently abrogated secretory granule fusion events. Taken together, our results suggest that $K_v2.1$ clusters act as a reservoir station to recruit large number of secretory granules from the cell interior, targeting them to Syn-3 via its C1b domain, which assists in conferring their status as newcomer secretory granules. This provides an efficient mechanism of distribution and replenishment of secretory granules to the newcomer secretory granule pool to affect part of first-phase GSIS and sustain most of second-phase GSIS.

Results

$K_v2.1$ increases insulin secretory granule fusions to promote biphasic GSIS

We assessed the endogenous function of $K_v2.1$ employing a reported and well-validated adeno-$K_v2.1$ shRNA (21), which could reduce the $K_v2.1$ expression in Wistar rat islets by 95% (Fig. 1*A*; see second experiment in Fig. S3*A*) and in rat β-cell line INS 832/13 (referred to herein as INS) by 89% (Fig. 1*B*, two experiments shown). Reduction of $K_v2.1$ expression did not significantly affect the levels of the indicated SNARE proteins (Fig. 1, *A* and *B*). Adeno-$K_v2.1$ shRNA treatment of Wistar islets resulted in inhibition of first-phase glucose (16.7 mM)-stimulated insulin secretion by 39% and second-phase GSIS by 32% (Fig. 1*C*). We then used a plasmid $K_v2.1$ shRNA/mCherry (shRNA directed at a reported rat sequence (22)) to infect INS cells, whereby mCherry-expressing cells were depleted of $K_v2.1$ (Fig. 1*D*, *bottom images*; *top images* show Ad-mCherry as control). We subjected the mCherry-positive INS cells to patch-clamp cell membrane capacitance (Cm) measurements (Fig. 1*E*) to assess single β-cell exocytosis. $K_v2.1$ depletion reduced total capacitance from 31.5 ± 3 fF/pF to 19 ± 2.5 fF/pF, which is a 40% reduction. Rescue of $K_v2.1$ expression (mouse sequence $K_v2.1$-EGFP) in $K_v2.1$-depleted cells (rat sequence) completely restored total capacitance to 35.6 ± 6.7 fF/PF (Fig. 1*E*).

To separate the effects of $K_v2.1$ on membrane potential *versus* exocytosis, we performed experiments measuring K_v current and Cm on untransfected INS cells and $K_v2.1$-overexpressing INS cells, before and after the application of stromatoxin (Alomone Labs, Jerusalem, Israel), a specific $K_v2.1$ current inhibitor (21). Overexpression of $K_v2.1$ greatly increased both K_v channel activity and exocytosis compared with control cells (Fig. 1*F*). In control INS cells, 100 nM stromatoxin strongly inhibited the K_v currents without affecting exocytosis. In $K_v2.1$-overexpressing INS cells, stromatoxin inhibited K_v current to a similar extent as control cells but also did not affect the potentiated exocytosis. These results indicate that in the condition whereby $K_v2.1$ effects on membrane excitability are fully inhibited, $K_v2.1$-mediated exocytosis remained intact and could still be increased by the $K_v2.1$-WT overexpression.

In addition, we performed current clamp ($I = 0$) to record membrane potential changes from control, $K_v2.1$-WT overexpression, and $K_v2.1$ KD mouse (C57Bl6) islet β-cells with 20 mM glucose stimulation, which showed no difference in the membrane potential increases between control ($n = 21$ cells), $K_v2.1$-WT ($n = 8$ cells), and $K_v2.1$ KD β-cells ($n = 7$ cells); representative traces are shown in Fig. S1*A*). This would suggest that the K_v channel contributing most to membrane potential changes in β-cells may not be $K_v2.1$ but rather $K_v2.2$; this may be in part due to $K_v2.2$ being much more abundant than $K_v2.1$ in β-cells (21). We also performed Ca_v current recordings (Fig. S1*B*) to assess for differences between control ($n = 9$ cells) and $K_v2.1$ KD β-cells ($n = 11$) and between control ($n = 15$ cells) and $K_v2.1$-WT overexpressing β-cells ($n = 13$) and also found no statistical differences.

The Goto–Kakizaki (GK) rat is a nonobese T2D diabetes model reported to have reduced islet levels of SNARE proteins (Syn-1A, SNAP25, and VAMP2) postulated to mediate fusion of predocked secretory granules, which in part explains the reduced first-phase GSIS typical of T2D (23). Fig. 2*A* confirmed the reduction in islet levels of Syn-1A (by 46%) and SNAP25 (by 88%) in GK rat islets compared with Wistar rat islets. In contrast, islet levels of Syn-3 (known to mediate newcomer secretory granule fusion) (18) were similar to Wistar rat islet levels. Remarkably, GK rat islet levels of $K_v2.1$ (but not $K_v2.2$; only nonsignificant 13% reduction) were reduced by 83%, suggesting that this might have contributed to the secretory deficiency of GK rat islets. In support, $K_v2.2$, which more recently purported to be the major contributor to K_v current in β-cells, was shown to have no effect on insulin secretion (21). To test this possibility, we overexpressed $K_v2.1$-WT (Ad-$K_v2.1$-WT) or its nonconducting pore mutant (Ad-$K_v2.1$-pore mutant W365C/Y380T) (6) into GK rat islets and performed an islet perifusion assay (Fig. 2*B*). Because the islet yield from GK rats isolation is low, we used INS to show the level of overexpression (Fig. 2*C*), which was 3-fold for $K_v2.1$-WT and 4-fold for $K_v2.1$-pore mutant, and both were sufficient in increasing the biphasic GSIS in GK rat islets by 51 and 45%, respectively (Fig. 2*B*).

Finally, we assessed the effects of shRNA-induced $K_v2.1$ depletion (Fig. 2*D*) and $K_v2.1$ overexpression (Fig. 2*E*) in INS cells at the level of single granule fusion by total internal reflection fluorescence microscopy (TIRFM). We used NPY-pHluorin and not NPY-EGFP to visualize secretory granule fusion, because we had aimed to determine *de novo* secretory granule fusion *per se* and their spatio-temporal relationships to the plasma membrane $K_v2.1$ clusters, and not to study the prefusion behavior of secretory granules (*i.e.* predocked secretory granules). NPY-pHluorin exocytosis in first phase will be largely from newcomer secretory granules but will also include some predocked secretory granules, whereas newcomer secre-

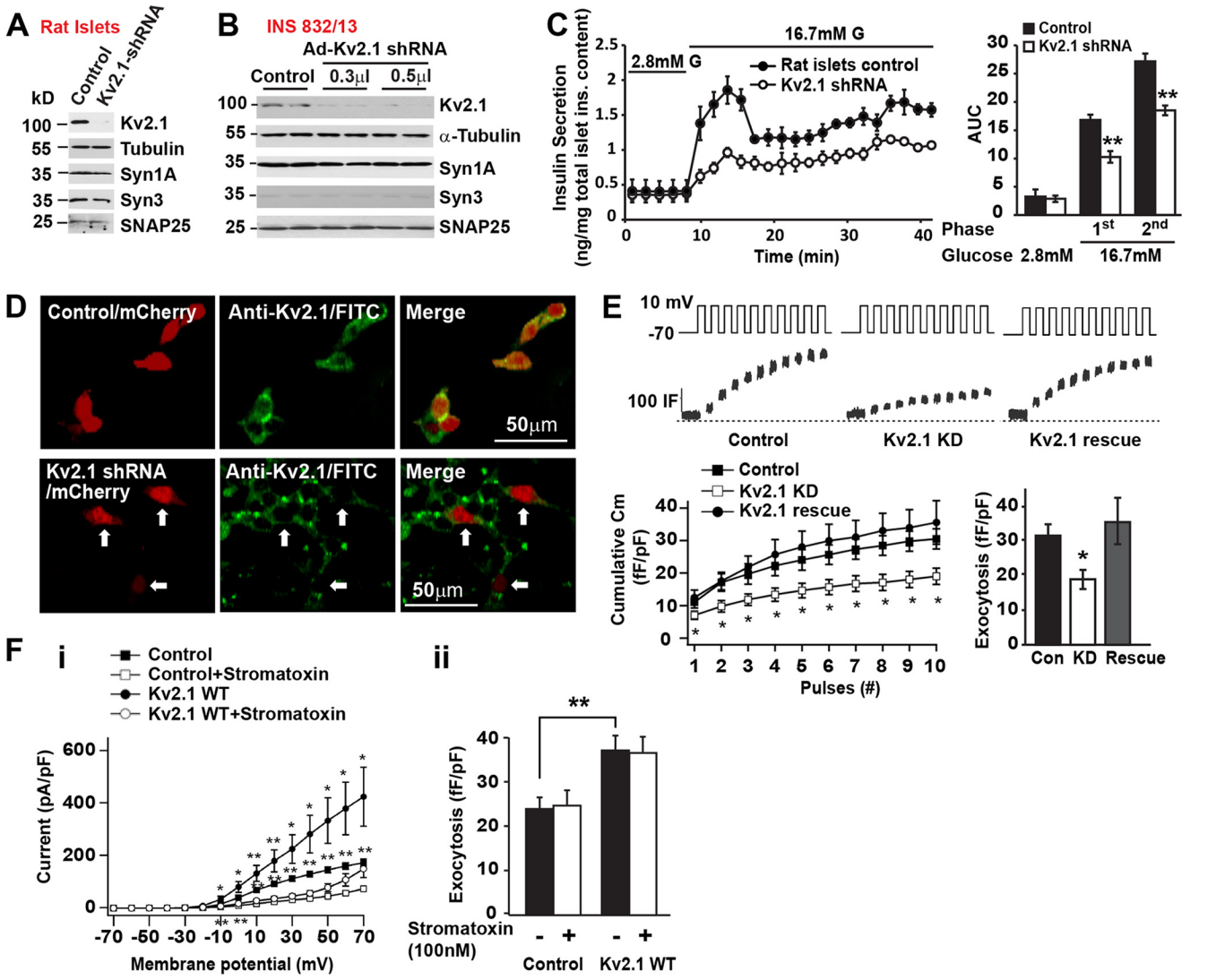

Figure 1. Depletion of $K_v2.1$ in β-cells reduces exocytosis of insulin secretory granules with the consequent inhibition of biphasic GSIS. *A* and *B*, Ad-$K_v2.1$ shRNA *versus* Ad-scrambled shRNA (as control) treatment of Wistar rat islets (*A*, representative of two separate experiments; second experiment is shown in Fig. S3*A*) and in INS 832/13 (*INS*) cells (*B*, two experiments run on the same blot) resulted in reduction of $K_v2.1$ expression. *C*, rat (Wistar) islet perifusion showing the effects of Ad-$K_v2.1$ shRNA *versus* Ad-scrambled shRNA treatments on biphasic GSIS. *AUC graph*, *first phase*, 11–23 min; *second phase*, 23–41 min; GSIS, $n = 3$, analyzed by independent-samples *t* test. *D* and *E*, patch-clamp Cm of INS cells transfected with pcDNA3-$K_v2.1$-shRNA/mCherry (rat sequence). The mCherry-expressing cells (indicated by *arrows*) showed reduction of $K_v2.1$ expression (*D*, *bottom images*) *versus* control PLKO-mCherry plasmid, showing abundant $K_v2.1$ (*D*, *top images*). *E*, rescue of $K_v2.1$ shRNA-mCherry with pcDNA3-$K_v2.1$-EGFP (mouse sequence) in INS cells. *Top*, representative recordings of a train of 500-ms depolarizations from −70 to 10 mV; *bottom left*, cumulative changes in Cm normalized to basal cell membrane capacitance (fF/pF); *bottom right*, total $Cm^{1st\text{-}10th}$ pulses, $n = 3$ experiments with 9–13 cells/group. *F*, separating the independent effects of $K_v2.1$ on K_v currents (*left*) and exocytosis (*right*); $n = 3$ experiments with 13–15 cells/group for *i* and $n = 13$ cells/group for *ii*. In control INS cells, stromatoxin (100 nM) inhibited K_v current but did not affect exocytosis. In $K_v2.1$-overexpressing INS cells, the greatly enhanced K_v currents were inhibited by stromatoxin to a similar extent as control INS cells, but the $K_v2.1$-enhanced increase in exocytosis was not affected by stomatoxin. All values in this figure represent mean ± S.E. (*error bars*); *, $p < 0.05$; **, $p < 0.01$.

tory granules will account for essentially all granule fusions in second phase (18, 24, 25). $K_v2.1$ depletion inhibited secretory granule exocytosis in first-phase (by 55%) and second-phase GSIS (by 70%; Fig. 2*D*). Conversely, $K_v2.1$-WT overexpression shown in Fig. 2*E* as normalized values to the "NPY-pHluorin control group" (values were normalized for comparison between experiments with different secretion rates) increased secretory granule fusion in the first (by 87%) and second phases (by 83%). This increase in secretory granule fusion by $K_v2.1$ overexpression is independent of its channel function because $K_v2.1$-pore mutant overexpression had effects in increasing secretory granule fusion very similar to those of $K_v2.1$-WT (Fig. 2*E*, *bottom*).

Spatial and functional relationships between insulin secretory granule fusion and β-cell plasma membrane $K_v2.1$ clusters

The above results prompted us to critically assess by TIRFM the spatio-temporal relationships between $K_v2.1$ channels on the β-cell plasma membrane and secretory granule fusion. Previous reports have shown that $K_v2.1$ channels insert into distinct plasma membrane microdomains to form clusters (9–11). In Fig. 3, we overexpressed $K_v2.1$-mCherry in INS cells, which indeed formed plasma membrane clusters. We co-expressed NPY-pHluorin to see where glucose-stimulated exocytosis occurs in relationship to the $K_v2.1$ clusters. We divided the entire surface area of the INS cell into an unbiased random grid

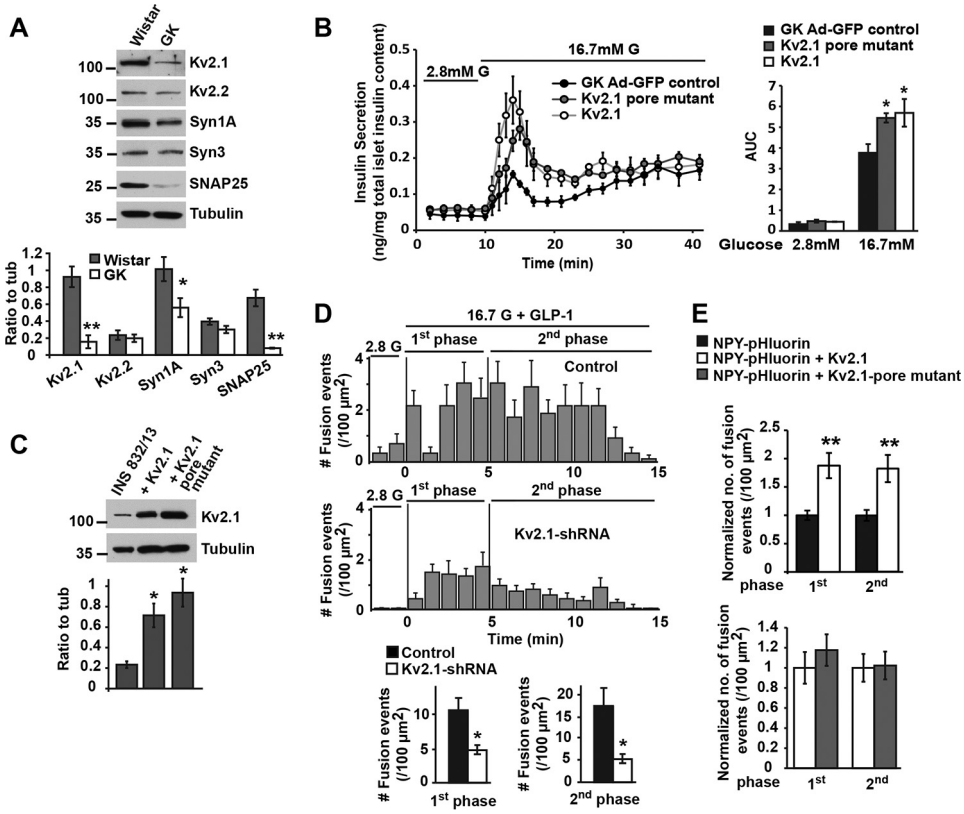

Figure 2. K_v2.1-WT or K_v2.1-pore mutant can potentiate insulin granule fusion with consequent enhancement of biphasic GSIS. *A*, GK rat islet levels of SNARE and K_v2.1 proteins. *Bottom graph*, summary of three experiments. *B*, Ad-K_v2.1-WT or Ad-K_v2.1-pore mutant overexpression in GK rat islets can rescue the deficient biphasic GSIS ($n = 3$). AUC analysis on the *right* is ANOVA with post hoc test for two-by-two comparisons. *C*, K_v2.1 overexpression in INS cells infected with Ad-K_v2.1-WT or Ad-K_v2.1-pore mutant. Ad-GFP infection of GK islets was used as a control. *Bottom graph*, summary of three experiments. *D*, depletion of K_v2.1 inhibits secretory granule fusion (Ad-NPY-pHluorin used to track granule fusion) in INS cells. Histograms show secretory granule fusion events in first (first 5 min after 16.7 mM glucose + 10 nM GLP-1 stimulation) and second phases (5–15 min) in control (*top*) *versus* K_v2.1 shRNA–treated cells (*middle*). *Bottom*, summary of secretory granule fusion in first and second phases ($n = 3$ experiments with 9–10 cells/group). *E*, K_v2.1 overexpression increases secretory granule fusion (first- and second-phase GSIS) that is independent of channel pore function. The number of fusion events of INS cells expressing NPY-pHluorin and K_v2.1-mCherry (*top*, *white bars*, $n = 6$ experiments with 28–32 cells/group) or K_v2.1-pore mutant-mCherry (*bottom*, *gray bars*, $n = 3$ experiments with 10 cells/group) was compared and normalized to cells expressing NPY-pHluorin only (*black bars*). All values in this figure represent mean ± S.E. (*error bars*); *, $p < 0.05$; **, $p < 0.01$.

of 5.12-μm^2 regions of interest (ROIs; Fig. 3 (*A* and *B*) shows INS cell in the midst of 18 mM glucose plus 10 nM GLP-1 stimulation). We defined "K_v2.1 cluster density" for each ROI as the averaged mCherry fluorescence over a 15-min acquisition time (see "Experimental procedures"). In that way, an ROI with more K_v2.1 clusters forming during the acquisition would show higher overall averaged fluorescence and be considered as having a higher "cluster density." After mCherry background fluorescence subtraction (see "Experimental procedures" and Fig. S2*A*), the secretory granule fusion events were counted and K_v2.1 cluster density was calculated for each ROI. To compare between cells with different numbers of fusion events and different mCherry fluorescence, for each cell, the values were normalized to the maximal number of fusion events and the maximal K_v2.1 cluster density value. We saw a positive correlation between the number of secretory granule fusion events and K_v2.1 cluster density (Fig. 3*C*). However, this correlation is independent of the channel electrical activity (Fig. 3, *D* and *E*) because expression of the K_v2.1-pore mutant had similar effects on the number of fusion events and in fact was slightly higher for the pore mutant (Fig. 3*E*). Measurements of the distance between fusion events and the nearest K_v2.1 cluster showed that secretory granule fusions appeared to occur mainly adjacent (distance of <2 μm) to the plasma membrane K_v2.1 clusters (Fig. 3*F*, *images*) and are also independent of channel electrical function, as K_v2.1-pore mutant clusters showed the same result (Fig. 3*F*, *graphs*). Specifically, there was no significant difference between the distance profiles (Fig. 3*F*, *left graph*) and the mean distances of granule fusions from the clusters (Fig. 3*F*, *right graph*) when comparing the K_v2.1-WT-mCherry and K_v2.1-pore mutant-mCherry clusters. Remarkably, about 60% of all secretory granule fusion events occurred within a 1-μm distance of a K_v2.1 cluster, and about 85% occurred within a 2-μm distance from the cluster; the number of fusion events decreased as the distance from K_v2.1 clusters increased. Whereas it was previously suggested that K_v2.1 is involved in insulin secretory granule exocytosis (6), this is the first time that the spatio-temporal relationship of secretory granule fusion to K_v2.1 is demonstrated. At very close examination (Fig. S2*B* shows two ROIs in representative high- and low-K_v2.1 cluster density areas), we saw more exocytotic events in the high-K_v2.1 cluster density areas (ROI in Fig. S2*B*, serial images of exocytosis in Fig. S2*C*, and corresponding K_v2.1-mCherry fluorescence trace in Fig. S2*E*) than the low-K_v2.1 cluster density areas (ROI 3 in Fig. S2*B*, serial images of exocytosis in Fig. S2*D*, and corresponding K_v2.1-mCherry fluorescence trace in Fig. S2*E*). For

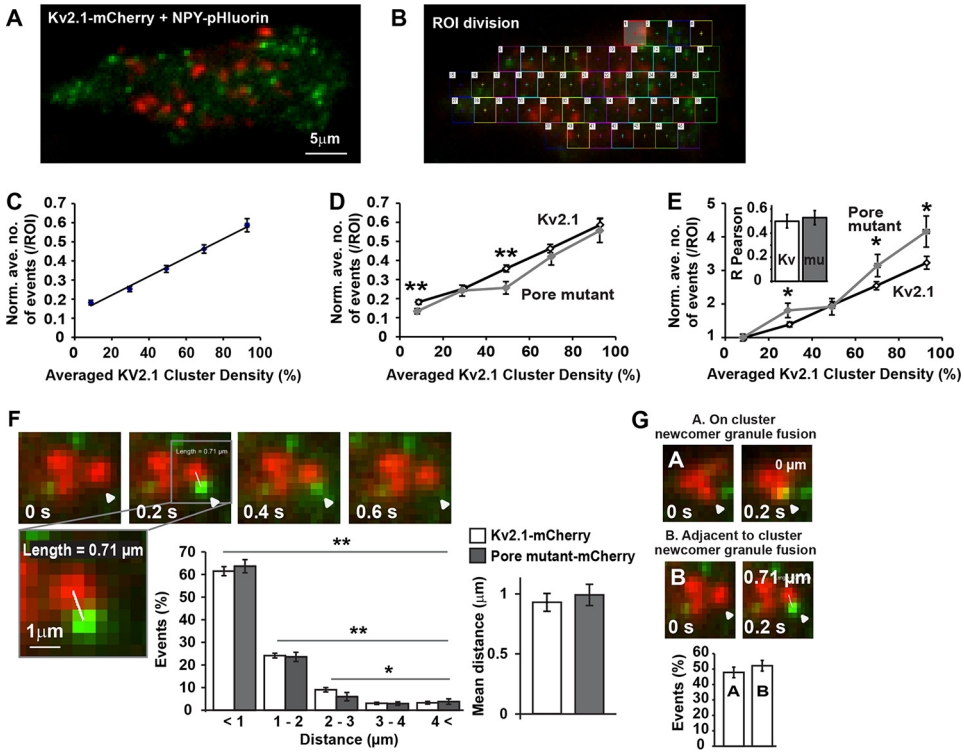

Figure 3. Spatial and functional relationships between insulin secretory granule fusion and $K_v2.1$ clusters on the β-cell plasma membrane. *A*, TIRFM imaging of stimulated (18 mM glucose + 10 nM GLP-1) INS cells cotransfected with $K_v2.1$-mCherry (*red*) and NPY-pHluorin (*green*). *B*, the same INS cell as in *A* with *grid division* drawn onto the entire plasma membrane surface into 5.12-μm^2 ROIs for analysis. *C*, positive correlation between the number of secretory granule fusion events and $K_v2.1$ cluster density. Shown is a summary of 25 cells from eight experiments. The values were normalized to the maximal value and averaged according to cluster density at 20% increments. *D* and *E*, positive correlation between the number of secretory granule fusion events and cluster density is independent of channel electrical function. *D*, comparison of "cluster density *versus* number of events" correlation between $K_v2.1$ (*black*) and $K_v2.1$-pore mutant (*gray*). *E*, change in the number of fusion events from baseline cluster density ($n = 3$ with 10 cells). *Inset*, no significant change in the Pearson correlation coefficients. *F*, secretory granule fusions occur adjacent to the $K_v2.1$ clusters and are independent of channel electrical function. *Top*, example of distance assessment (see *enlarged image*, *bottom*) between a secretory granule fusion event (*green*, *top* serial images showing newcomer secretory granule fusion) and nearest $K_v2.1$-mCherry cluster (*red*), which is indicated by the *white diagonal bar* drawn from the center of the $K_v2.1$ cluster to the *center* of the insulin granule. *Left graph*, correlation between percentage of fusion events and distance from the nearest $K_v2.1$-mCherry (*white*; $n = 8$ with 25 cells) or $K_v2.1$-pore mutant-mCherry (*gray*; $n = 3$ with 10 cells) cluster. *Right graph*, mean distance from nearest $K_v2.1$-mCherry (*white*; $n = 3$ with 11 cells) or $K_v2.1$-pore mutant-mCherry (*gray*; $n = 3$ with 11 cells) cluster. *G*, analysis of fusion events at distance <1 μm. An "on-cluster" secretory granule fusion event is considered to be within a distance of 0–0.5 μm, as shown in *A*, and an "adjacent-to-cluster" secretory granule fusion is considered to be within a distance of 0.5–1 μm, as shown in *B*. *Bottom*, comparison of the percentage of fusion events that were "on" clusters and "adjacent to" clusters. All values in this figure represent mean ± S.E. (*error bars*); *, $p < 0.05$; **, $p < 0.01$.

secretory granule fusion events that are <1-μm distant from a $K_v2.1$ cluster, about 50% are "on" the $K_v2.1$ clusters (distance of 0–0.5 μm), and 50% are "adjacent to" the $K_v2.1$ clusters (distance 0.5–1 μm; Fig. 3*G*). Whereas some of the effects described above might be due to $K_v2.1$ overexpression, we assumed that $K_v2.1$-mCherry subunits, which have been functionally tested by electrophysiology (see Fig. 5), would dimerize with the endogenous $K_v2.1$ to form the tetrameric channel structure (26).

Syntaxin-3 interactions with distinct C1 domains within $K_v2.1$ form $K_v2.1$-SNARE excitosome complexes

Syntaxin (Syn)-3 is the dominant syntaxin that mediates fusion of newcomer secretory granules (18) in contrast to Syn-1A purported to prefer predocked insulin secretory granules (27). We assessed what excitosome complex Syn-3 would be forming with $K_v2.1$ in INS cells, compared with Syn-1A (Fig. 4*A*; Fig. S3*B* shows another representative blot of three). $K_v2.1$-C1 pulled down both Syn-1A and Syn-3, VAMP2, and SNAP25. We also verified this, employing the HEK293 expression system (Fig. 4*B*; Fig. S3*C* shows another representative blot of three). Our results are consistent with previous reports showing SNAP25 and VAMP2 binding to the $K_v2.1$ N terminus (28, 29).

We then critically assessed Syn-3 *versus* Syn-1A binding to $K_v2.1$ C1 domains. It was previously reported that Syn-1A preferentially binds strongly to the C1a domain of $K_v2.1$ (3, 30) and weakly to the $K_v2.1$ N terminus (31). In contrast, we found that Syn-3 preferentially binds the C1b domain and not C1a. This was shown in Fig. 4*C*, whereby GST-$K_v2.1$-C1a binding to expressed Syn-3 was superior to GST-$K_v2.1$-C1b (equal loading inputs of GST proteins shown as Ponceau S staining in Fig. S2*D*). This was confirmed in Fig. 4*D*, showing that full-length $K_v2.1\Delta$C1a (intact C1b) bound full-length GST-Syn-3 strongly, whereas full-length $K_v2.1\Delta$C1b (intact C1a) binding to GST-Syn-3 was very weak. We then assessed the major binding domain within Syn-3 and found that the cytoplasmic H3 domain also preferentially binds $K_v2.1\Delta$C1a and with similarly reduced binding to $K_v2.1\Delta$C1b. Similarly, the H3 domain of Syn-1A has been shown to be the "business" end of the syntaxin that binds cognate SNARE proteins (16). It therefore appears

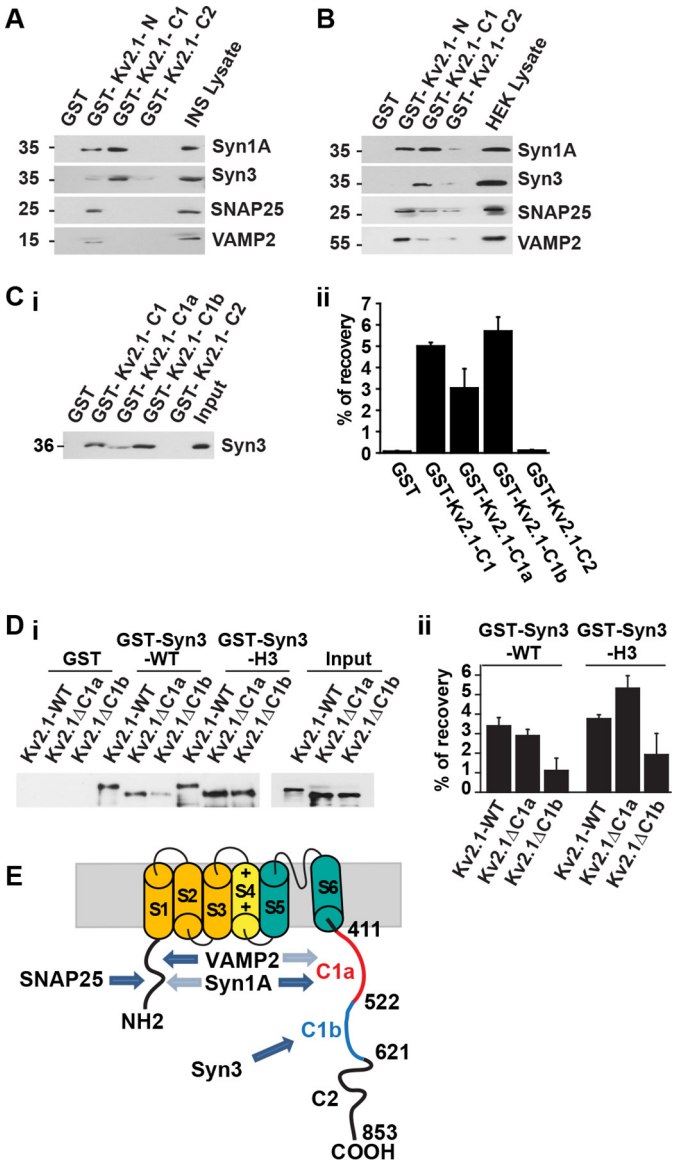

Figure 4. Syntaxin-3 interactions with distinct C1 domains within $K_v2.1$ form a $K_v2.1$-SNARE excitosome complex. *A*, endogenous SNARE proteins from INS cells bind different cytoplasmic domains of $K_v2.1$ (C1, aa 411–621; C2, aa 622–853; N, aa 1–186). *B*, overexpressed SNARE proteins in HEK293 cells bind different cytoplasmic domains of $K_v2.1$. For VAMP2, we used VAMP2-EGFP to obtain clearer signals, which explains the larger molecular weight. *A* and *B*, representative blot of three separate experiments. A second experiment for *A* and *B* is shown in Fig. S3 (*B* and *C*). *C*, GST (as control) and GST-$K_v2.1$-C1, -C1a (aa 411–522), -C1b (aa 523–621), or -C2, all bound to GSH-agarose beads, were used to pull down Syn-3 from the lysate extract of HEK293 cells transfected with Syn-3. *i*, representative blot of three separate experiments. *ii*, mean ± S.E. (*error bars*) summary results from three experiments. Ponceau S staining of a blot to demonstrate the similar amounts of GST fusion proteins loaded is shown in Fig. S3*D*. *D*, Syn-3-WT and its cytoplasmic H3 domain bind to distinct ΔK$_v$2.1-C1a (deletion of aa 411–522) or -ΔC1b (deletion of aa 523–621). *i*, representative blot of three separate experiments, with the equal inputs shown on the *right*. Ponceau S staining of the blot to demonstrate the similar amounts of GST proteins loaded is shown in Fig. S2*E*. *ii*, summary of densitometry scanning of the specific bands from the three experiments. The results are expressed as mean ± S.E., and values normalized to the percentage of recovery from the cell lysate extract (500 μg of protein) were used for the binding (inputs shown in *i* (*right*)). *E*, a schematic showing where these different SNARE proteins bind to the different cytoplasmic domains of $K_v2.1$. *Dark blue arrows*, strong binding; *light blue arrows*, weaker binding.

that newcomer secretory granule SNARE protein Syn-3 binds a $K_v2.1$ domain that is distinct from predocked secretory granule SNARE protein Syn-1A (model in Fig. 4*E*).

Syntaxin-3 affects β-cell $K_v2.1$ channels by regulating current amplitudes

We then assessed the functional consequences of the $K_v2.1$ C1a and C1b deletions. $K_v2.1$ mutant plasmids with deletion of C1a ($K_v2.1\Delta C1a$) or C1b ($K_v2.1\Delta C1b$) were expressed in HEK293 cells to assess which of these $K_v2.1$ domains affects channel activity, and then we assessed which was acted on by Syn-3. Compared with $K_v2.1$ (1343 ± 235 pA/pF, $n = 9$; Fig. 5*A*), $K_v2.1\Delta C1a$ completely lost channel function with maximum current density of only 52 ± 6 pA/pF ($n = 9$; Fig. 5*B*), similar to the current density of $K_v2.1$-pore mutant (94 ± 22 pA/pF, $n = 6$; Fig. 5*B*). $K_v2.1\Delta C1b$ showed a more moderate reduction of maximum current density to 631 ± 142 pA/pF ($n = 11$; Fig. 5*B*), compared with $K_v2.1\Delta C1a$. When cells were cotransfected with Syn-3 and $K_v2.1$ or $K_v2.1\Delta C1a$ or $K_v2.1\Delta C1b$, Syn-3 greatly reduced $K_v2.1$ current (549 ± 183 pA/pF; $n = 7$; Fig. 5*A*) but would not further reduce the currents of $K_v2.1\Delta C1b$ (Fig. 5*C*). The effect of Syn-3 on $K_v2.1\Delta C1a$ current could not be determined because the channel completely lost its function to conduct current. Nonetheless, when taken together with the binding study in Fig. 4, Syn-3 probably affects $K_v2.1$ channel function *per se* by acting on its C1b domain.

To test the effect of $K_v2.1$ depletion on K_v current in INS cells, cells were transfected with control shRNA/mCherry or $K_v2.1$ shRNA/mCherry (rat sequence) plasmids. Depletion of endogenous rat $K_v2.1$ greatly reduced K_v current amplitude from the maximum current density of 184 ± 19 pA/pF (control, $n = 9$ cells) to 96 ± 15 pA/pF ($K_v2.1$ shRNA–treated, $n = 9$ cells (Fig. 5*D*), a 48% reduction) but did not affect calcium influx (data not shown). To confirm that the reduction in currents of $K_v2.1$-depleted cells was indeed attributable to $K_v2.1$ *per se*, the depleted cells were transfected with $K_v2.1$-EGFP (mouse sequence). Restoration of $K_v2.1$ expression into $K_v2.1$-depleted cells rescued K_v current by 89% (180 ± 19 pA/pF, $n = 10$; $p < 0.01$) or to 98% of control INS cells (Fig. 5*D*). Finally, we deleted endogenous Syn-3 in INS cells (Fig. 5*E*), which caused a 46% increase in K_v current from the maximum K_v current amplitudes of 171 ± 14 pA/pF (control; $n = 9$) to 249 ± 19 pA/pF (Syn-3 shRNA–treated; $n = 9$). Taken along with Fig. 5*A*, these results indicate that the increased K_v current was attributed to $K_v2.1$ channels, although it was previously reported (21) that $K_v2.2$ ($K_v2.2$ shown to be present in INS in Fig. 2*A*) could have also contributed.

Distinct $K_v2.1$ C1a/b domains have different effects on insulin granule fusion, which include the spatial relationship of granule fusion to $K_v2.1$ clusters

We generated $K_v2.1$ domain deletions (ΔC1a, ΔC1b) of full-length $K_v2.1$ and tagged these constructs with mCherry (flanked by linkers) at the first extracellular domain between S1 and S2 (Fig. 6*A*). We confirmed by electrophysiology the functional $K_v2.1$ currents of these internally tagged $K_v2.1$ constructs (Fig. 5). We examined the expression of these constructs in INS

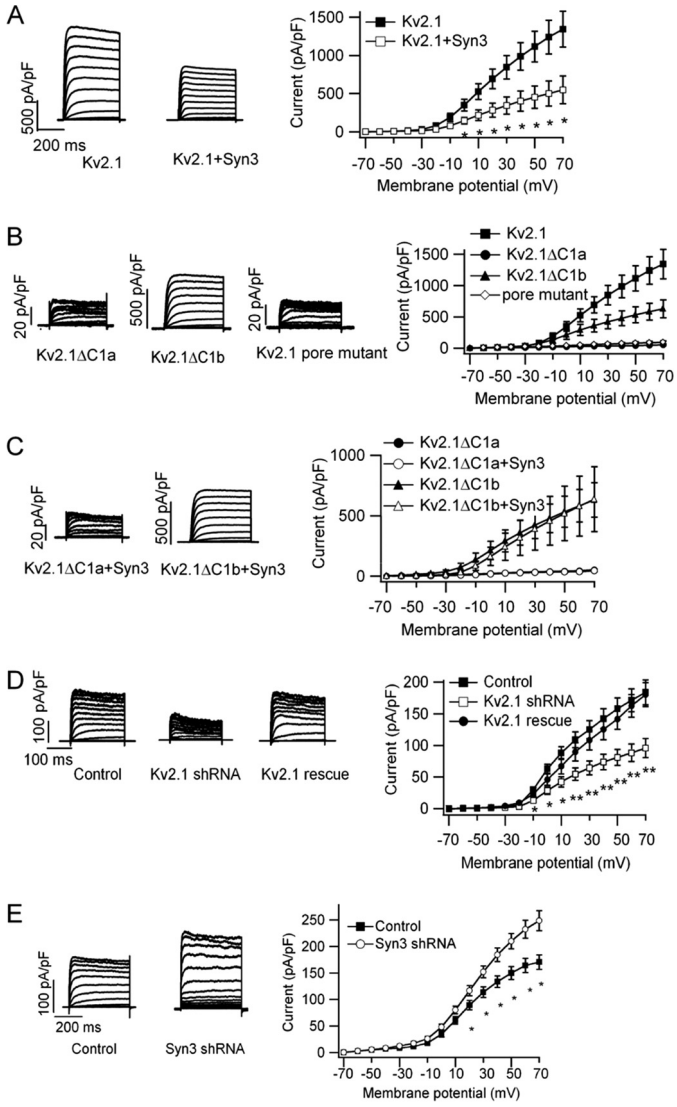

Figure 5. Syntaxin-3 affects β-cell $K_v2.1$ currents. *A*, Syn-3 overexpression in HEK293 cells inhibited the current amplitude of co-expressed $K_v2.1$. *Left*, representative whole-cell currents of $K_v2.1$ without or with Syn-3; *Right*, current-voltage relationship of $K_v2.1$ without ($n = 9$ cells) or with Syx-3 ($n = 7$ cells). Currents were normalized by cell capacitance to yield current density. Values are means ± S.E. (*error bars*); *, $p < 0.05$. *B* and *C*, comparison of current amplitudes of $K_v2.1$ and $K_v2.1$-pore mutant (in *B*) and also $K_v2.1\Delta C1a$ and $K_v2.1\Delta C1b$ without (*B*) and with Syn-3 co-expression (in *C*) in HEK293 cells ($n = 10–11$ cells). *D*, K_v current, reduced by $K_v2.1$ depletion in INS cells, can be rescued by $K_v2.1$ restoration. *Left*, representative K_v currents in INS cells infected with control shRNA/mCherry (control), $K_v2.1$ shRNA/mCherry ($K_v2.1$ shRNA–treated), or $K_v2.1$ shRNA/mCherry plus $K_v2.1$-EGFP ($K_v2.1$ rescue). *Right*, current–voltage relationship. Values are means ± S.E. ($n = 9–10$ cells). *, $p < 0.05$; **, $p < 0.01$; control *versus* $K_v2.1$ shRNA–treated cells or rescue of $K_v2.1$ shRNA–treated cells. *E*, Syn-3 depletion in INS cells by shRNA treatment increased K_v current amplitudes. *Left*, representative K_v currents from control/mCherry and Syn-3 shRNA/mCherry–treated INS cells. *Right*, current–voltage relationships; shRNA control ($n = 9$ cells) and Syn-3 shRNA ($n = 9$ cells).

cells, which showed that the deletions did not exhibit significant changes in the number and size of the $K_v2.1$ clusters (Fig. 6*B*, *left* and *middle*) and overall $K_v2.1$ mCherry fluorescence intensity (Fig. 6*B*, *right*). Remarkably, $K_v2.1\Delta C1b$-mCherry expression completely reversed the potentiating effects of $K_v2.1$ on first- and second-phase secretory granule fusion (Fig. 6*C*; the number of fusion events in each category was normalized to control value of NPY-pHluorin only). In contrast, despite some nonsignificant trend, $K_v2.1\Delta C1a$-mCherry expression did not affect $K_v2.1$-potentiating effects on secretory granule fusions in first phase or second phase. We then assessed whether $K_v2.1\Delta C1a$ or $K_v2.1\Delta C1b$ would influence the distance between the secretory granule fusion events and the $K_v2.1$ clusters (Fig. 6*D*). Indeed, both $K_v2.1\Delta C1b$ (stronger effects) and $K_v2.1\Delta C1a$ expression (albeit weaker effects) showed significantly fewer fusion events that were directly adjacent to $K_v2.1$ clusters (distance <1 μm) and more fusion events that were farther off the $K_v2.1$ clusters, thus considered as "off-cluster" (distance >4 μm). We examined the correlation between the number of fusion events and $K_v2.1$ channel cluster density. In contrast to $K_v2.1$-WT, which showed low fusion events in the low-$K_v2.1$ cluster density areas (Fig. 3, *C–E*), both $K_v2.1\Delta C1a$-mCherry (Fig. S4*A*, ROI 3; corresponding mCherry fluorescence trace in Fig. S4*B* and serial images in Fig. S4*D*) and $K_v2.1\Delta C1b$-mCherry (Fig. S4*E*, ROI 3; corresponding mCherry fluorescence trace in Fig. S3*F* and serial images in Fig. S4*H*) showed increased fusion events in areas of low $K_v2.1$ cluster density (Fig. 6*E*, *left*). At high $K_v2.1$ cluster density, $K_v2.1\Delta C1a$-mCherry increased secretory granule fusions (Fig. S4*A*, ROI 2; corresponding mCherry fluorescence trace in Fig. S4*B* and serial images at Fig. S4*C*) similar to $K_v2.1$-WT. However, secretory granule fusions with $K_v2.1\Delta C1b$-mCherry (Fig. 6*E*, *left*) were low (Fig. S4*E*, ROI 2; corresponding mCherry fluorescence trace in Fig. S4*F* and serial images in Fig. S4*G*) and in fact showed no correlation between secretory granule fusion and $K_v2.1$ cluster density (Fig. 6*E*, *middle* and *right*). As indicated, this was better depicted in representative 5–7-min acquisition fluorescent traces in Fig. S4 for $K_v2.1\Delta C1a$-mCherry (*A–D*) and $K_v2.1\Delta C1b$-mCherry (*E–H*) compared with $K_v2.1$-mCherry (Fig. S2, *B–E*). These results of the effects of C1b deletion indicate that the C1b domain of $K_v2.1$ is a/the major putative domain influencing the relationship of insulin secretory granule fusion to changes in plasma membrane $K_v2.1$ cluster density.

Discussion

Our work suggests that the large amount of $K_v2.1$ clusters on the β-cell plasma membrane (12, 13) may in part serve to recruit secretory granules via Syn-3 (mainly newcomer secretory granules (18)) to this physical reservoir. This would suggest that the plasma membrane $K_v2.1$ clusters probably serve as a reservoir for both Syn-3 and secretory granules to continually feed the releasable pools after their depletion from glucose-stimulated secretion, particularly during the second phase. This might in part also explain why the great majority (almost 85%) of secretory granule fusions (almost all newcomer secretory granules in second phase) were within 2 μm of a plasma membrane $K_v2.1$ cluster, whereas only 10–15% of fusion events occur distal to $K_v2.1$ clusters. In fact, L-type Ca^{2+} channels were found to co-localize to the plasma membrane $K_v2.1$ clusters in neurons (15). More work will be needed to assess the distribution and spatial relationships between the different putative Ca^{2+} channels and $K_v2.1$ clusters and the spatio-temporal behavior of secretory granules and Syn-3 from their postulated release from the $K_v2.1$ cluster reserve pool to the Ca_v/SNARE excitosome fusion sites (8, 32) (see below).

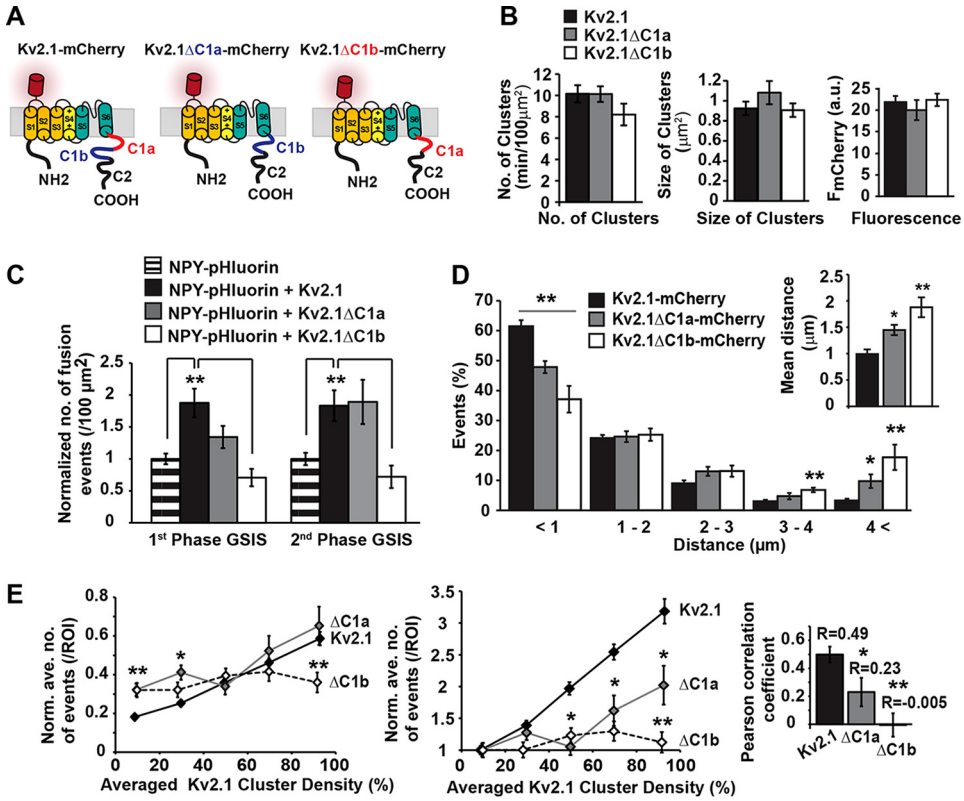

Figure 6. Distinct K_v2.1 C1a/b domains have different effects on secretory granule fusion and its relationship to the K_v2.1 clusters. *A*, schematic description of K_v2.1 domain deletion constructs. *B*, comparison of K_v2.1/K_v2.1ΔC1a/K_v2.1ΔC1b-mCherry cluster formation (*black*/*gray*/*white*, respectively); number of clusters (*left*), size of clusters (*middle*), and overall mCherry fluorescence (*right*) ($n = 3$ with 15–17 cells). *C*, C1b deletion reverses the effect of K_v2.1 on secretory granule fusion. Number of secretory granule fusion events normalized to cells expressing NPY-pHluorin only (*striped*, as control), compared with cells expressing NPY-pHluorin and K_v2.1-mCherry (*black*) or K_v2.1ΔC1a-mCherry (*gray*) or K_v2.1ΔC1b-mCherry (*white*, $n = 3$ with 10–11 cells, one-way ANOVA Bonferroni test). *D*, changes in the profile of "secretory granule fusion distance from K_v2.1 clusters" caused by the K_v2.1 domain deletions. Shown is a percentage of fusion events (*main graph*) and mean distance from the nearest cluster (*top inset*) comparison of K_v2.1-mCherry (*black*), K_v2.1ΔC1a-mCherry (*gray*), and K_v2.1ΔC1b-mCherry (*white*; $n = 3$ with 10–11 cells, one-way ANOVA Bonferroni test). *E*, correlation between the number of fusion events and K_v2.1 cluster density was impaired in K_v2.1ΔC1a-mCherry and completely abolished in K_v2.1ΔC1b-mCherry. *Left*, comparison of "cluster density *versus* number of fusion events" correlation between K_v2.1-mCherry (*black*), K_v2.1ΔC1a-mCherry (*gray*) and K_v2.1ΔC1b-mCherry (*white*). *Middle*, comparison of the change in the number of fusion events from baseline K_v2.1 cluster density of the three constructs ($n = 3$ with 10–11 cells). *Right*, change in the Pearson correlation coefficients. All values in this figure represent mean ± S.E. (*error bars*). *, $p < 0.05$; **, $p < 0.01$.

How do K_v2.1 clusters distribute secretory granules to the newcomer secretory granule pools for fusion? Adjacent C1a and C1b domains of K_v2.1 bind Syn-1A (3), which mediates predocked secretory granule fusion (27), and Syn-3 (this study), which mediates newcomer secretory granule fusion, respectively (18). Here, we showed that deletion of the C1b domain of K_v2.1 selectively reduced secretory granule fusions, the great majority tracked by the NPY-pHluorin to be newcomer secretory granules, particularly during second-phase GSIS. Moreover, after the C1b deletion, more fusion events appeared to be distant (particularly >4 μm) from K_v2.1 clusters (*i.e.* off clusters) (Fig. 6*D*). Because K_v2.1 C1a binds Syn-1A (3), this would in part explain the milder (insignificant) effects of C1a deletion (Fig. 6, *C–E*) that probably affected predocked granules that contributed to first phase GSIS. Thus, we postulate that Syn-3 (this work) and Syn-1A (3, 6) would also serve to specifically shepherd secretory granules from the K_v2.1 clusters to the adjacent Ca^{2+} channels. Why are there far fewer fusions at the off-cluster sites? We speculate a combination of reasons. There might be reduced population of Ca^{2+} channels or lesser abundance of SNARE proteins at these off-cluster plasma membrane sites. The third, perhaps more important, reason would be that after the depletion of secretory granules after stimulated fusion at these off-cluster sites, they cannot be replenished by the "on-cluster" reservoir of secretory granules located so far from these exocytotic sites. Thus, insulin secretory granules exocytosis at the off-cluster sites are much less efficient than at the on-cluster sites.

We found that Syn-3 also had direct effects on K_v2.1 channel current, redundant to the effects of Syn-1A (31). This raises the possibility that Syn-1A–K_v2.1 and Syn-3–K_v2.1 complexes might have distinct effects on the microdomains affecting membrane excitability. This finding, taken together with our recent report that Syn-3 also regulates L- and R-type Ca^{2+} channels (32), led us to think that the resulting differences in membrane microdomain electrical and ion properties might contribute to the distinct fusion readiness of predocked (16) *versus* newcomer secretory granules, the latter observed to be better primed for fusion (18). Although Syn-3 binding and impairment of K_v2.1 channel activity would be expected to reduce plasma membrane potential, which would predictably desensitize the β-cell-to-glucose stimuli, hence inducing some inhibition of GSIS, it seems that these effects of Syn-3 on K_v2.1 channel activity were greatly superseded by Syn-3/K_v2.1 effects

on promoting insulin granule exocytosis. This thinking is supported by three findings. First, the potentiating effects of the $K_v2.1$-pore mutant on insulin granule exocytosis were similar to those of $K_v2.1$-WT. Second, stromatoxin inhibition of $K_v2.1$ electrical activity had little to no effect on $K_v2.1$-mediated exocytosis. Third, $K_v2.1$ knockdown or overexpression's effects on membrane potential were not different from those of control, and neither $K_v2.1$ knockdown nor overexpression had significant effects on Ca_v currents. An alternative explanation is that the reduced $K_v2.1$ channel activity might have been compensated by $K_v2.2$, which is abundant in both rodent (21) and human β cells (33). In fact, in the report by MacDonald and co-workers (33), $K_v2.2$ was 10 times more abundant than $K_v2.1$, and whereas both K_v values contributed to outward current in β cells, only $K_v2.1$ knockdown and not $K_v2.2$ knockdown in both human β-cells and INS cells impaired depolarization-induced exocytosis. Perhaps the electrical activity mediated by intact $K_v2.2$ is sufficient to compensate or override $K_v2.1$'s contribution, when $K_v2.1$ is perturbed either by knockdown or overexpression.

Our current results are in complete agreement with findings from two other laboratories. The groups of both Lotan (3–5) and MacDonald (33) had shown that $K_v2.1$ has an exocytosis function that is not related to the channel pore *per se* and is localized to the channels' C terminus (3, 33). The most recent report by MacDonald and co-workers (33), in part using static TIRFM analysis, had assessed the effects of $K_v2.1$ knockdown and overexpression in both INS and human β-cells, including type-2 diabetes human β-cells; those results were uniformly consistent with the thinking that $K_v2.1$ supported glucose-dependent recruitment of insulin granules for exocytosis. Consistent with the results of MacDonald and co-workers (33), our work employing real-time TIRFM and Cm showed that $K_v2.1$ overexpression in INS cells increased $K_v2.1$ channel density and exocytosis and could rescue biphasic GSIS in T2D GK rat islets. The report of MacDonald and co-workers (33) focused on the role of Syn-1A and predocked granule fusion and employed a large C-terminal deletion of 318 amino acids. This deletion includes C1a (aa 411–522), which binds Syn-1A (3); the C2 domain (aa 621–853), which is not known to bind a SNARE protein (and which we show here to not bind Syn-3); and, interestingly, also half of the C1b domain at aa 536–621. This is in contrast to our work here showing that the C1b domain (aa 522–621) *per se* binds Syn-3. Whereas both works share similar conclusions regarding the role of $K_v2.1$ clusters in the plasma membrane, the major novel contribution of our work is the discovery of how these $K_v2.1$ clusters specifically serve as physical reservoirs to regulate newcomer insulin granule recruitment and subsequent fusion through its interaction with Syn-3; the latter we had previously demonstrated to mediate newcomer granule fusion (18).

Our laboratory and others have contributed much work with regard to the exocytotic steps that come after secretory granules are released from the reserve pool, including insulin granule docking, priming, and fusion that involve SNARE, priming, and other accessory proteins (reviewed in Refs. 17 and 34). Of note, $K_v2.1$'s role in exocytosis is not at the secretory granule fusion apparatus *per se*, but rather in the form of $K_v2.1$ clusters in the plasma membrane, which we here propose serve as a reserve pool that enables delivery of granules to sit in this pool near the plasma membrane, awaiting mobilization to the releasable pools when stimulated. The size of releasable pools of granules available for fusion is largely determined by the full capacity of the docking/fusion machinery *per se*, which is regulated by the assembly and disassembly of SNARE and priming fusion proteins and other accessory factors (*i.e.* calcium sensors) (16, 17, 34). Little is known about the factors that mobilize granules from the reserve pool to the releasable pools, and even less is known about the reserve pool. In T2D islets, the amounts of many but not all of the SNARE and priming proteins are reduced (20, 23, 35). In our recent report (35), we showed that Syn-3 and cognate VAMP8 are not reduced in T2D human islets, which could conceivably respond in extracting more granules from the $K_v2.1$ overexpression–induced enlargement of the reserved pool to replenish the newcomer granules sufficient to rescue GSIS but only to near normal levels.

Last, T2D islets showed profound reduction in $K_v2.1$ levels (21), whereby a consequent declustering of $K_v2.1$ would predictably reduce its secretory granule reservoir function. This would in turn reduce the capacity to replenish the pools of newcomer secretory granules (this study) and probably also predocked secretory granules, particularly after glucose-stimulated depletion. Intriguingly, we showed that biphasic GSIS in diabetic GK rat islets could be restored to normal levels by the $K_v2.1$ overexpression without having to replenish the deficient SNARE protein fusion machinery. Similarly, MacDonald's group (33) showed that $K_v2.1$ overexpression could also rescue the deficient GSIS from human T2D islets. These two examples of rescue of T2D islets by $K_v2.1$ suggest that secretory granule replenishment to releasable pools from the plasma membrane $K_v2.1$ cluster reservoir could at least partially compensate for the deficiency in the SNARE complex fusion apparatus (20). This is perhaps because the smaller amounts of β-cell SNARE proteins could potentially undergo more efficient cycles of disassembly and reassembly, provided that a continued supply of secretory granules is made available. Nonetheless, we showed that the rescue of GSIS did not overshoot normal levels because the effects of the $K_v2.1$ overexpression were on the reserve or reservoir pools and not on the releasable pools that are still affected by the deficient docking and fusion machinery attributed to deficiency of SNARE and priming proteins and other accessory proteins (20, 23).

Experimental procedures

Molecular biology

Full-length mouse $K_v2.1$ cDNA, purchased from OriGene Technologies Co., was amplified and subcloned into pCDNA3 expression plasmid using BamHI and NotI restriction enzymes. mCherry and EGFP fluorescent protein, flanked by linkers, were fused extracellularly to $K_v2.1$ between S1 and S2 transmembrane segments using transfer-PCR restriction-free cloning as described (36). $K_v2.1$ deletions and pore mutant (W365C/Y380T (6) for rat and the corresponding W369C/Y384T for mouse) were generated on the basis of the aforementioned chosen construct using site-directed mutagenesis. $K_v2.1$

shRNA-mCherry plasmid was purchased from VectorBiolab on the basis of a reported rat $K_v2.1$ shRNA sequence (22). Adeno-$K_v2.1$ shRNA virus was kindly donated by Mette Jensen and Chris Newgard (Duke University) (21). Adeno-$K_v2.1$-WT (Ad-$K_v2.1$-WT) and its nonconducting pore mutant (Ad-$K_v2.1$-pore mutant W365C/Y380T (6)) were gifts from Joss Manning-Fox and Patrick MacDonald (University of Edmonton).

Animals and pancreatic islet isolation

Male GK rats (10–12 weeks old, original colony obtained from Karolinska Institute, Stockholm, Sweden) (35) were housed in an environmentally controlled room with a 12-h/12-h light/dark cycle and allowed *ad libitum* access to standard rat chow and water. Age-matched male Wistar rats (Charles River Laboratories, Montreal, Canada) served as controls. Animals were cared for and housed in accordance with Canadian Council on Animal Care Standards and the Animals for Research Act of Ontario. Animals were sacrificed by overdose of isoflurane inhalation followed by islet isolation. All procedures were approved by the University of Toronto Faculties of Medicine and Pharmacy Animal Care Committee.

Pancreatic islets of Langerhans were isolated and cultured in RPMI1640 medium with 10% FBS as described previously (35). We are able to obtain an average of 150 islets/GK rat and 500 islets/Wistar rat. About 100 islets/rat are required for each lane of the Western blotting study and 50 islets per perifusion chamber for the perifusion assay. Each experiment (each N) was from a different rat. However, we have tried our best to reduce the number of animals used. For example, for a GK rat islet isolation yielding 150 islets, we would use 100 islets for the Western blotting study and 50 islets for the perifusion assay.

In vitro binding assay and immunoblotting

In vitro binding assays were performed according to the methods we described previously (37). Briefly, GST (as control) and the indicated GST proteins (Syn-3-WT, $K_v2.1$ domains) (250 pmol of protein each) were bound to GSH-agarose beads and incubated with the lysate extracts of INS cells or HEK293 cells transfected with the indicated SNARE proteins or full-length $K_v2.1$-WT-mCherry or its C1a- or C1b-truncated mutants. These beads and lysates were then incubated in lysis buffer (50 mM Tris (pH 7.4), 150 mM NaCl, 1.5% Triton X-100, 1 μg/ml pepstatin A, 1 μg/ml leupeptin, and 10 μg/ml aprotinin) at 4 °C for 2 h with constant agitation. The beads were then washed three times with lysis buffer, and the samples were then separated on 10–12% SDS-PAGE and transferred to nitrocellulose membrane, and the proteins of interest were identified with the specific antibodies. The blots were quantified by densitometry scanning followed by analysis with ImageJ.

Western blot analysis

Rat β-cell line INS 832/13 (here referred to as INS cells) or rat islets were infected with Ad-$K_v2.1$ shRNA virus. 48 h after infection, the cells and islets were collected, and the cell lysate were separated on 12–15% gradient SDS-PAGE and transferred to nitrocellulose membrane, and the proteins of interest were identified with specific primary antibodies against $K_v2.1$ (1:100) and $K_v2.2$ (1:800) (both from Alomone Labs), tubulin (1:5000; Sigma), Syn-1A (1:1000) and Syn-3 (1:1000) (both from Synaptic Systems), and VAMP2 (1:2000) and VAMP8 (1:250) (both from R&D Systems).

Electrophysiology

Patch-clamp recordings were performed on HEK293 and INS cells using an EPC-10 amplifier and Pulse software (HEKA Electronik, Lambrecht, Germany). Recording pipettes were pulled by a Sutter P-97 puller (Sutter Inc., Novato, CA) from 1.5-mm glass tubes and were fire-polished to a resistance of 1.5–2 megaohms when filled with pipette solution. The pipette solution for $K_v2.1$ current recording contained 140 mM KCl, 1 mM $MgCl_2$, 1 mM EGTA, 10 mM HEPES, and 5 mM MgATP (pH 7.4-adjusted with KOH). The external bath solution contained 140 mM NaCl, 4 mM KCl, 1 mM $MgCl_2$, 2 mM $CaCl_2$, 10 mM HEPES, and 10 mM glucose (pH 7.3 with NaOH). After a whole-cell configuration was established, membrane potential was held at −70 mV and depolarized for 250 ms from −70 to +70 mV in 10-mV increments. Maximum current was divided by cell membrane capacitance to calculate current density (pA/pF) to normalize current size across different cells. For measurement of membrane capacitance, the intracellular solution contained 125 mM cesium glutamate, 10 mM CsCl, 10 mM NaCl, 1 mM $MgCl_2$, 5 mM HEPES, 0.05 mM EGTA, 3 mM MgATP, and 0.1 mM cAMP (pH 7.4). The extracellular solution consisted of 118 mM NaCl, 5.6 mM KCl, 1.2 mM $MgCl_2$, 10 mM $CaCl_2$, 20 mM tetraethylammonium chloride, 5 mM HEPES, and 5 D-glucose (pH 7.4). Cm was estimated by the Lindau–Neher technique, implementing the "Sine-DC" feature of the Lock-in module (40 mV peak-to-peak and a frequency of 500 Hz) in the whole-cell configuration. Exocytic events were elicited by a train of 10 500-ms depolarization pulses (1-Hz stimulation frequency) from −70 to 10 mV. Current data were recorded at room temperature (22–24 °C), and Cm data were record at 30 °C.

Confocal immunofluorescence microscopy

Immunostaining was performed with primary antibody rabbit anti-$K_v2.1$ (Alomone Labs) and secondary antibody anti-rabbit FITC. Immunostained cells mounted on glass coverslips were examined using a laser-scanning confocal imaging system (LSM510) equipped with LSM software (Carl Zeiss, Oberkochen, Germany) using a ×63 oil objective and 488- and 543-nm excitation lasers for fluorescein isothiocyanate and mCherry, respectively.

TIRFM imaging and analysis

TIRFM images were acquired using a Nikon Eclipse Ti-E inverted microscope with Perfect Focus system and taken at 17 MHz with 100-ms exposure time and collected with an Andor DU-897 Ultra camera. INS cells were transfected with different combinations of plasmids 2 days before the experiment (38, 39) and imaged in imaging buffer (20 mM HEPES, 5 mM NaCl, 140 mM potassium gluconate, 2 mM $MgCl_2$, and 2.8 mM glucose buffer pre-equilibrated with O_2/CO_2 (95:5), pH 7.4) (40). Transfected cells were excited simultaneously with 488- and

561-nm lasers to excite neuropeptide Y (NPY)-pHluorin and mCherry, respectively, and imaged with Dualview filters to separate red and green signals. The images were acquired at 200-ms intervals for 2 min in rest conditions (2.8 mM glucose) and an additional 15 min with glucose stimulation (18 mM glucose + 10 nM GLP-1). Fusion events, observed as flashes of fluorescence with dissipation wider than initial diameter indicating emptying of the NPY-pHluorin cargo, were manually selected. Exocytosis of secretory granules was analyzed using NIS-Elements imaging software. For correlation between $K_v2.1$ cluster density and calculation of the number of fusion events, we followed the following protocol. Each cell was grid-divided into 5.12-μm^2 ROIs, and then the background of each cell, defined as the ROI with the lowest mCherry intensity, was subtracted from all other ROIs. $K_v2.1$-mCherry clusters within each ROI were identified as dynamic red masses with a minimum size of 0.5 μm^2 and intensity above the background threshold (Fig. S2*A*, *right*), $K_v2.1$ cluster density was then calculated as averaged intensity of mCherry within the ROI. The number of fusion events within the ROI was counted over 15-min acquisition times (Fig. S2 (*B–E*) for representative 5-min recordings). ROIs with higher "$K_v2.1$ cluster density" showed more $K_v2.1$ cluster dynamic formation over time and thus had higher mCherry intensity levels (Fig. S2, *C* and *E*) compared with ROIs with lower "$K_v2.1$ cluster density" (Fig. S2, *D* and *E*). The cells had strong mCherry intensity; therefore, there was no significant mCherry photobleaching observed. Because the cells vary in the number of fusion events and mCherry fluorescence intensity, both values were normalized to the maximum value of each cell. The normalized values of $K_v2.1$ cluster density were plotted *versus* the normalized number of fusion events. Then the Spearman correlation coefficient was calculated. For averaged correlation from all cells, the normalized values from all cells were collected and averaged according to five quantified $K_v2.1$ cluster density ranges: 0–20, 20–40, 40–60, 60–80, and 80–100%. For the measurements of distances of fusion events from the $K_v2.1$ clusters, clusters were defined after background subtraction, as indicated above. The distance was measured from the center of the fusion event to the center of the nearest $K_v2.1$ cluster (for clusters smaller than 0.64 μm^2) or 0.45 μm into the nearest cluster (for clusters larger than 0.64 μm^2). All TIRFM experiments were performed at 37 °C.

Islet perifusion and insulin secretion assays

Batches of 50 rat islets loaded into perifusion chambers were stimulated with 16.7 mM glucose as reported previously (19), with secreted insulin measured by RIA (EMD Millipore). Insulin secreted was always normalized to total islet insulin content to negate the bias of islet size and β-cell number.

Statistical analysis

All data are presented as mean ± S.E. Statistical significance was evaluated by Student's *t* test, one-way ANOVA Bonferroni test, and bivariate correlation Pearson test using SPSS software. Significant differences are indicated by asterisks (*, $p < 0.05$; **, $p < 0.01$).

Author contributions—D.G.-A., L.X., T.Q., H.X., D.Z., S.D., T.L., Y.K., and H.Y.G. conceptualization; D.G.-A., Y.H., and H.Y.G. resources; D.G.-A., L.X., T.Q., H.X., D.Z., S.D., T.L., A.B.H., Y.K., and H.Y.G. data curation; D.G.-A., L.X., and Y.K. software; D.G.-A., L.X., T.Q., D.Z., S.D., T.L., Y.K., and H.Y.G. formal analysis; D.G.-A., L.X., T.Q., H.X., D.Z., S.D., T.L., Y.K., and H.Y.G. validation; D.G.-A., Y.H., and H.Y.G. investigation; D.G.-A., L.X., T.Q., H.X., D.Z., S.D., T.L., Y.K., and H.Y.G. visualization; D.G.-A., L.X., T.Q., H.X., D.Z., S.D., T.L., A.B.H., Y.K., and H.Y.G. methodology; D.G.-A., L.X., T.Q., D.Z., S.D., Y.K., and H.Y.G. writing-original draft; D.G.-A., L.X., F.K., and H.Y.G. writing-review and editing; H.Y.G. supervision; H.Y.G. funding acquisition; H.Y.G. project administration.

Acknowledgments—Some equipment used in this study was supported by the 3D (Diet, Digestive Tract, and Disease) Centre funded by Canadian Foundation for Innovation and Ontario Research Fund, project number 19442. We thank Jocelyn Manning-Fox and Patrick MacDonald (University of Alberta) and Christopher Newgard and Mette Jensen (Duke University) for providing the adenoviruses.

References

1. Jacobson, D. A., Kuznetsov, A., Lopez, J. P., Kash, S., Ammälä, C. E., and Philipson, L. H. (2007) $K_v2.1$ ablation alters glucose-induced islet electrical activity, enhancing insulin secretion. *Cell Metab.* **6,** 229–235 CrossRef Medline
2. MacDonald, P. E., Sewing, S., Wang, J., Joseph, J. W., Smukler, S. R., Sakellaropoulos, G., Wang, J., Saleh, M. C., Chan, C. B., Tsushima, R. G., Salapatek, A. M., and Wheeler, M. B. (2002) Inhibition of $K_v2.1$ voltage-dependent K^+ channels in pancreatic beta-cells enhances glucose-dependent insulin secretion. *J. Biol. Chem.* **277,** 44938–44945 CrossRef Medline
3. Singer-Lahat, D., Sheinin, A., Chikvashvili, D., Tsuk, S., Greitzer, D., Friedrich, R., Feinshreiber, L., Ashery, U., Benveniste, M., Levitan, E. S., and Lotan, I. (2007) K^+ channel facilitation of exocytosis by dynamic interaction with syntaxin. *J. Neurosci.* **27,** 1651–1658 CrossRef Medline
4. Feinshreiber, L., Singer-Lahat, D., Ashery, U., and Lotan, I. (2009) Voltage-gated potassium channel as a facilitator of exocytosis. *Ann. N.Y. Acad. Sci.* **1152,** 87–92 CrossRef Medline
5. Feinshreiber, L., Singer-Lahat, D., Friedrich, R., Matti, U., Sheinin, A., Yizhar, O., Nachman, R., Chikvashvili, D., Rettig, J., Ashery, U., and Lotan, I. (2010) Non-conducting function of the Kv2.1 channel enables it to recruit vesicles for release in neuroendocrine and nerve cells. *J. Cell Sci.* **123,** 1940–1947 CrossRef Medline
6. Dai, X. Q., Manning Fox, J. E., Chikvashvili, D., Casimir, M., Plummer, G., Hajmrle, C., Spigelman, A. F., Kin, T., Singer-Lahat, D., Kang, Y., Shapiro, A. M., Gaisano, H. Y., Lotan, I., and Macdonald, P. E. (2012) The voltage-dependent potassium channel subunit $K_v2.1$ regulates insulin secretion from rodent and human islets independently of its electrical function. *Diabetologia* **55,** 1709–1720 CrossRef Medline
7. Sheng, Z. H., Rettig, J., Cook, T., and Catterall, W. A. (1996) Calcium-dependent interaction of N-type calcium channels with the synaptic core complex. *Nature* **379,** 451–454 CrossRef Medline
8. Wiser, O., Trus, M., Hernández, A., Renström, E., Barg, S., Rorsman, P., and Atlas, D. (1999) The voltage sensitive Lc-type Ca^{2+} channel is functionally coupled to the exocytotic machinery. *Proc. Natl. Acad. Sci. U.S.A.* **96,** 248–253 CrossRef Medline
9. O'Connell, K. M., and Tamkun, M. M. (2005) Targeting of voltage-gated potassium channel isoforms to distinct cell surface microdomains. *J. Cell Sci.* **118,** 2155–2166 CrossRef Medline
10. O'Connell, K. M., Rolig, A. S., Whitesell, J. D., and Tamkun, M. M. (2006) $K_v2.1$ potassium channels are retained within dynamic cell surface microdomains that are defined by a perimeter fence. *J. Neurosci.* **26,** 9609–9618 CrossRef Medline
11. Baver, S. B., and O'Connell, K. M. (2012) The C-terminus of neuronal $K_v2.1$ channels is required for channel localization and targeting but not

for NMDA-receptor-mediated regulation of channel function. *Neuroscience* **217,** 56–66 CrossRef Medline
12. O'Connell, K. M., Loftus, R., and Tamkun, M. M. (2010) Localization-dependent activity of the $K_V2.1$ delayed-rectifier K^+ channel. *Proc. Natl. Acad. Sci. U.S.A.* **107,** 12351–12356 CrossRef Medline
13. Fox, P. D., Loftus, R. J., and Tamkun, M. M. (2013) Regulation of $K_V2.1$ K^+ conductance by cell surface channel density. *J. Neurosci.* **33,** 1259–1270 CrossRef Medline
14. Deutsch, E., Weigel, A. V., Akin, E. J., Fox, P., Hansen, G., Haberkorn, C. J., Loftus, R., Krapf, D., and Tamkun, M. M. (2012) $K_V2.1$ cell surface clusters are insertion platforms for ion channel delivery to the plasma membrane. *Mol. Biol. Cell* **23,** 2917–2929 CrossRef Medline
15. Fox, P. D., Haberkorn, C. J., Akin, E. J., Seel, P. J., Krapf, D., and Tamkun, M. M. (2015) Induction of stable ER-plasma-membrane junctions by $K_V2.1$ potassium channels. *J. Cell Sci.* **128,** 2096–2105 CrossRef Medline
16. Südhof, T. C., and Rothman, J. E. (2009) Membrane fusion: grappling with SNARE and SM proteins. *Science* **323,** 474–477 CrossRef Medline
17. Gaisano, H. Y. (2014) Here come the newcomer granules, better late than never. *Trends Endocrinol. Metab.* **25,** 381–388 CrossRef Medline
18. Zhu, D., Koo, E., Kwan, E., Kang, Y., Park, S., Xie, H., Sugita, S., and Gaisano, H. Y. (2013) Syntaxin-3 regulates newcomer insulin granule exocytosis and compound fusion in pancreatic beta cells. *Diabetologia* **56,** 359–369 CrossRef Medline
19. Zhu, D., Zhang, Y., Lam, P. P., Dolai, S., Liu, Y., Cai, E. P., Choi, D., Schroer, S. A., Kang, Y., Allister, E. M., Qin, T., Wheeler, M. B., Wang, C. C., Hong, W. J., Woo, M., and Gaisano, H. Y. (2012) Dual role of VAMP8 in regulating insulin exocytosis and islet beta cell growth. *Cell Metab.* **16,** 238–249 CrossRef Medline
20. Ostenson, C. G., Gaisano, H., Sheu, L., Tibell, A., and Bartfai, T. (2006) Impaired gene and protein expression of exocytotic soluble *N*-ethylmaleimide attachment protein receptor complex proteins in pancreatic islets of type 2 diabetic patients. *Diabetes* **55,** 435–440 CrossRef Medline
21. Jensen, M. V., Haldeman, J. M., Zhang, H., Lu, D., Huising, M. O., Vale, W. W., Hohmeier, H. E., Rosenberg, P., and Newgard, C. B. (2013) Control of voltage-gated potassium channel $K_V2.2$ expression by pyruvate-isocitrate cycling regulates glucose-stimulated insulin secretion. *J. Biol. Chem.* **288,** 23128–23140 CrossRef Medline
22. Jiao, S., Liu, Z., Ren, W. H., Ding, Y., Zhang, Y. Q., Zhang, Z. H., and Mei, Y. A. (2007) cAMP/protein kinase A signalling pathway protects against neuronal apoptosis and is associated with modulation of $K_V2.1$ in cerebellar granule cells. *J. Neurochem.* **100,** 979–991 CrossRef Medline
23. Gaisano, H. Y., Ostenson, C. G., Sheu, L., Wheeler, M. B., and Efendic, S. (2002) Abnormal expression of pancreatic islet exocytotic soluble *N*-ethylmaleimide-sensitive factor attachment protein receptors in Goto-Kakizaki rats is partially restored by phlorizin treatment and accentuated by high glucose treatment. *Endocrinology* **143,** 4218–4226 CrossRef Medline
24. Shibasaki, T., Takahashi, H., Miki, T., Sunaga, Y., Matsumura, K., Yamanaka, M., Zhang, C., Tamamoto, A., Satoh, T., Miyazaki, J., and Seino, S. (2007) Essential role of Epac2/Rap1 signaling in regulation of insulin granule dynamics by cAMP. *Proc. Natl. Acad. Sci. U.S.A.* **104,** 19333–19338 CrossRef Medline
25. Seino, S., Takahashi, H., Fujimoto, W., and Shibasaki, T. (2009) Roles of cAMP signalling in insulin granule exocytosis. *Diabetes Obes. Metab.* **11,** 180–188 CrossRef Medline
26. Grizel, A., Popinako, A., Kasimova, M. A., Stevens, L., Karlova, M., Moisenovich, M. M., and Sokolova, O. S. (2014) Domain structure and conformational changes in rat KV2.1 ion channel. *J. Neuroimmune Pharmacol.* **9,** 727–739 CrossRef Medline
27. Ohara-Imaizumi, M., Fujiwara, T., Nakamichi, Y., Okamura, T., Akimoto, Y., Kawai, J., Matsushima, S., Kawakami, H., Watanabe, T., Akagawa, K., and Nagamatsu, S. (2007) Imaging analysis reveals mechanistic differences between first- and second-phase insulin exocytosis. *J. Cell Biol.* **177,** 695–705 CrossRef Medline
28. MacDonald, P. E., Wang, G., Tsuk, S., Dodo, C., Kang, Y., Tang, L., Wheeler, M. B., Cattral, M. S., Lakey, J. R., Salapatek, A. M., Lotan, I., and Gaisano, H. Y. (2002) Synaptosome-associated protein of 25 kilodaltons modulates $K_V2.1$ voltage-dependent K^+ channels in neuroendocrine islet beta-cells through an interaction with the channel N terminus. *Mol. Endocrinol.* **16,** 2452–2461 CrossRef Medline
29. Lvov, A., Chikvashvili, D., Michaelevski, I., and Lotan, I. (2008) VAMP2 interacts directly with the N terminus of $K_V2.1$ to enhance channel inactivation. *Pflugers Arch.* **456,** 1121–1136 CrossRef Medline
30. Tsuk, S., Michaelevski, I., Bentley, G. N., Joho, R. H., Chikvashvili, D., and Lotan, I. (2005) $K_V2.1$ channel activation and inactivation is influenced by physical interactions of both syntaxin 1A and the syntaxin 1A/soluble *N*-ethylmaleimide-sensitive factor-25 (t-SNARE) complex with the C terminus of the channel. *Mol. Pharmacol.* **67,** 480–488 Medline
31. Leung, Y. M., Kang, Y., Gao, X., Xia, F., Xie, H., Sheu, L., Tsuk, S., Lotan, I., Tsushima, R. G., and Gaisano, H. Y. (2003) Syntaxin 1A binds to the cytoplasmic C terminus of $K_V2.1$ to regulate channel gating and trafficking. *J. Biol. Chem.* **278,** 17532–17538 CrossRef Medline
32. Xie, L., Dolai, S., Kang, Y., Liang, T., Xie, H., Qin, T., Yang, L., Chen, L., and Gaisano, H. Y. (2016) Syntaxin-3 binds and regulates both R- and L-type calcium channels in insulin-secreting INS 832/13 cells. *PLoS One* **11,** e0147862 CrossRef Medline
33. Fu, J., Dai, X., Plummer, G., Suzuki, K., Bautista, A., Githaka, J. M., Senior, L., Jensen, M., Greitzer-Antes, D., Manning Fox, J. E., Gaisano, H. Y., Newgard, C. B., Touret, N., and MacDonald, P. E. (2017) $K_V2.1$ clustering contributes to insulin exocytosis and rescues human beta-cell dysfunction. *Diabetes* **66,** 1890–1900 CrossRef Medline
34. Gaisano, H. Y. (2017) Recent new insights into the role of SNARE and associated proteins in insulin granule exocytosis. *Diabetes Obes. Metab.* **19,** 115–123 CrossRef Medline
35. Qin, T., Liang, T., Zhu, D., Kang, Y., Xie, L., Dolai, S., Sugita, S., Takahashi, N., Ostenson, C. G., Banks, K., and Gaisano, H. Y. (2017) Munc18b increases insulin granule fusion, restoring deficient insulin secretion in type-2 diabetes human and Goto-Kakizaki rat islets with improvement in glucose homeostasis. *EBioMedicine* **16,** 262–274 CrossRef Medline
36. Erijman, A., Dantes, A., Bernheim, R., Shifman, J. M., and Peleg, Y. (2011) Transfer-PCR (TPCR): a highway for DNA cloning and protein engineering. *J. Struct. Biol.* **175,** 171–177 CrossRef Medline
37. Pasyk, E. A., Kang, Y., Huang, X., Cui, N., Sheu, L., and Gaisano, H. Y. (2004) Syntaxin-1A binds the nucleotide-binding folds of sulphonylurea receptor 1 to regulate the KATP channel. *J. Biol. Chem.* **279,** 4234–4240 CrossRef Medline
38. Chao, C., Liang, T., Kang, Y., Lin, X., Xie, H., Feng, Z. P., and Gaisano, H. Y. (2011) Syntaxin-1A inhibits KATP channels by interacting with specific conserved motifs within sulfonylurea receptor 2A. *J. Mol. Cell Cardiol.* **51,** 790–802 CrossRef Medline
39. Liang, T., Xie, L., Chao, C., Kang, Y., Lin, X., Qin, T., Xie, H., Feng, Z. P., and Gaisano, H. Y. (2014) Phosphatidylinositol 4,5-biphosphate (PIP2) modulates interaction of syntaxin-1A with sulfonylurea receptor 1 to regulate pancreatic beta-cell ATP-sensitive potassium channels. *J. Biol. Chem.* **289,** 6028–6040 CrossRef Medline
40. Kang, Y., Zhang, Y., Liang, T., Leung, Y. M., Ng, B., Xie, H., Chang, N., Chan, J., Shyng, S. L., Tsushima, R. G., and Gaisano, H. Y. (2011) ATP modulates interaction of syntaxin-1A with sulfonylurea receptor 1 to regulate pancreatic beta-cell KATP channels. *J. Biol. Chem.* **286,** 5876–5883 CrossRef Medline